International Journal of Fracture **48**: 103–114, 1991.

Relationships between fracture parameters and fracture surface roughness of brittle polymers

K. ARAKAWA and K. TAKAHASHI
Research Institute for Applied Mechanics, Kyushu University, Kasuga-shi, 816 Japan

Received 10 May 1989; accepted in revised form 30 January 1990

Abstract. Fracture parameters such as crack velocity $\dot{a}$, stress intensity factor K_d and a specific crack extension resistance R^* were measured for Homalite-100, PMMA and epoxy in the course of fast crack propagation using a Cranz-Schardin type high speed camera. Fracture surface roughness λ was evaluated as a function of crack length a so that it could be correlated with the fracture parameters above. The results showed that none of those parameters could be uniquely related to λ. Instead, there was a good correlation between λ and a product $R^*\dot{a}$.

1. Introduction

When fracture velocity $\dot{a}$ becomes higher in brittle polymers, fracture surfaces generally tend to be rougher. The surfaces are occasionally referred to with such words as "mirror", "mist" and "hackle" according to the roughness changes from smooth to rough [1, 2]. The change should have a closer relationship with dynamic fracture procedures. Some attempts were made to correlate fracture parameters with the roughness. Cotterell [3, 4] measured surface roughness λ for poly(methyl methacrylate) (PMMA) and correlated it with $\dot{a}$. His study showed that λ increased as $\dot{a}$ increased. Recently, Ravi-Chandar and Knauss [5] measured K_d and $\dot{a}$ in Homalite-100 using the method of caustics. They obtained a result that showed λ increased consistently with the increase of K_d. However, as far as quantitative correlation of λ with other fracture parameters is concerned, only a few results have been published up to the present. This seems to be mostly due to the fact that considerably large scatter is involved in values of fracture parameters obtained from experiments, which makes it hard to show the correlation more explicitly.

The purpose of the present work was to study dependence of the fracture roughness on fracture parameters for brittle polymers. Attention was focused particularly on whether the roughness could be uniquely related with a single parameter such as $\dot{a}$ and K_d. Our recent experimental study for tensile plates of Araldite D and PMMA yielded a result that demonstrated that the relation between $\dot{a}$ and K_d was not unique [6]. Roughness measurement was expected to provide some hints for a physical meaning of the nonuniqueness, because the roughness was considered to reflect substantially the extent of material resistance, or fracture toughness, in the dynamic stress field ahead of a propagating crack tip. The same specimen geometry was adopted in the present study as the one in the previous work [6]. Specimens of Homalite-100 were studied because this material had been frequently used as a model material for dynamic fracture experiments. Specimens of Araldite D and PMMA were also studied to confirm results of Homalite-100.

2. Specimens and experimental procedure

Experiments were performed on single-edge-cracked tensile specimens of Homalite-100, PMMA (Acrylite S-001) and Araldite D. The specimen geometry, which is the same as the one in the previous work [6], is shown in Fig. 1. It was 120 mm in length and 150 mm in width. The thicknesses were 3.2 mm for Homalite-100, 5 mm for PMMA and epoxy. A sharp precrack was generated by momentum-controlled chisel impact onto a premachined saw-cut on a specimen edge. The specimens were eccentrically pin-loaded as shown in Fig. 1. The axis of the tensile loading was so eccentrically chosen that attainable peak fracture velocities could be variable to a certain extent; the loading axis was at a location which was 10 to 30 mm internally apart from the initial crack tip position. Because of the specimen geometry stated above, cracks could experience both acceleration and deceleration stages in one fracture process [6]. The specimens were loaded at a cross-head speed of 1 mm min^{-1} on an Instron type tensile machine under room temperature.

Mechanical and optical properties of the specimen materials are listed in Table 1. The elastic constants were evaluated under dynamic conditions by measuring velocities of longitudinal and shear ultrasonic waves (400 kHz), where well-known elastic relationships [7] between the wave velocities and the elastic constants were used. Dynamic stress-optical constants were determined through experiments for Homalite-100 and epoxy, whereas a

Table 1. Material and optical properties

		Homalite-100	PMMA	Araldite D
c_1	$m\,s^{-1}$	2598	2540	2600
c_2	$m\,s^{-1}$	1240	1415	1170
E_d	GPa	5.11	5.97	4.39
G_d	GPa	1.89	2.43	1.60
ν_d		0.35	0.28	0.37
ρ	$kg\,m^{-3}$	1230	1187	1170
c^*	$m^2\,N^{-1}$	7.67×10^{-11}	4.9×10^{-11}	7.0×10^{-11}
K_c	$MN\,m^{-3/2}$	0.41	1.20	0.64
R_c	$N\,m^{-1}$	32.9	241.2	93.3

c_1: longitudinal wave speed, c_2: shear wave speed, E_d: Young's modulus, G_d; shear modulus, ν_d: Poisson's ratio, ρ: density, c^*: stress-optical constant, K_c: stress intensity factor for an arresting crack, R_c: crack extension resistance for an arresting crack.

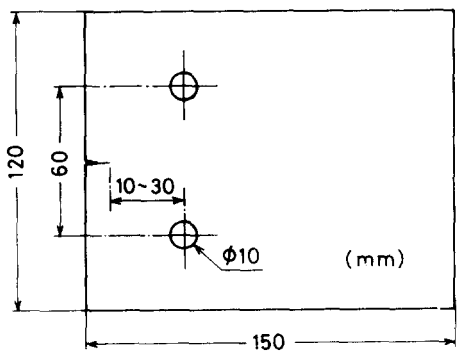

Fig. 1. Specimen geometry.

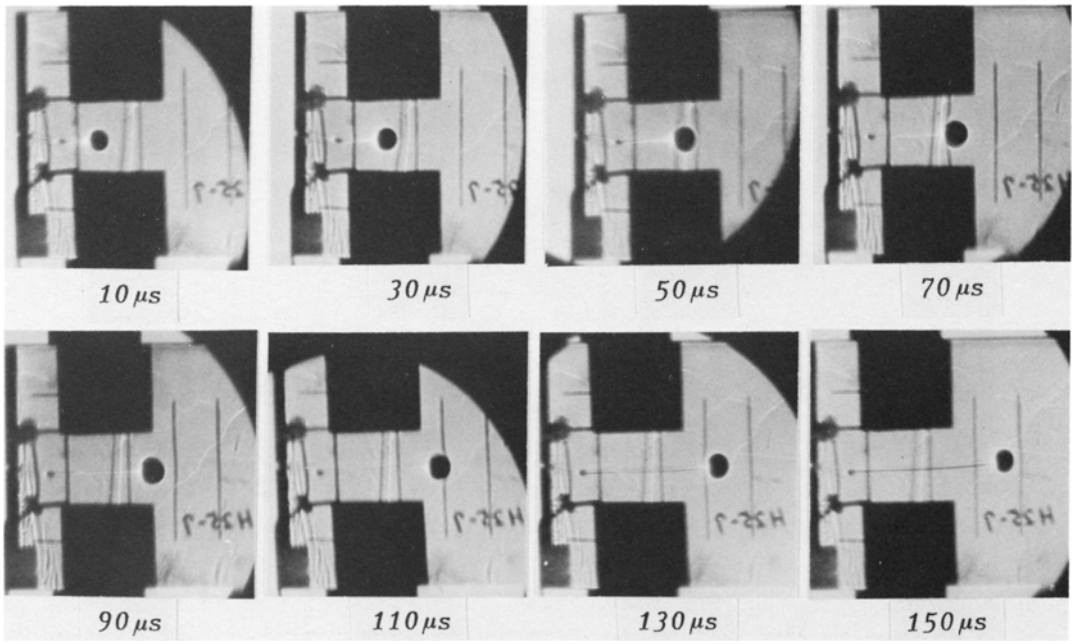

Fig. 2. Caustic patterns during dynamic crack propagation in Homalite-100.

value for PMMA was cited from the literature [8]. The K_c and R_c are the stress intensity factor and the crack extension resistance for a crack at arrest, respectively. We employed the shadow optical method of caustics to evaluate K_d and K_c during crack propagation, where a Cranz–Shardin type high speed camera [6] was used. The camera had 30 frames and worked at a framing rate from 1 to 10^6 frames s^{-1}. Figure 2 shows examples of shadow patterns for a fast crack in a Homalite-100 specimen. It is worth noting that the size of the caustics increased in an early stage of crack propagation and then decreased. This is typical fracture behaviour in the eccentrically pin-loaded specimens [6]. The stress intensity factor K_d or K_c was evaluated from the following equation [9]:

$$K_d = (2\sqrt{2\pi}/3z_0 dc\eta^{3/2})(\phi/3.17)^{5/2}, \quad (1)$$

where ϕ is the caustic diameter, z_0 is a distance between the specimen and the image plane, d is the specimen thickness and η is a convergency factor for incident light rays.

Figure 3 shows variations of K_d and a versus time t. In order to minimize data scattering in evaluation of fracture parameters, we employed a data-fitting procedure [6]; obtained values of K_d and a were expressed as ninth order polynomials of t based on the least square method so that they fitted their observed values most closely. Values of $\dot{a}$ and $\ddot{a}$ were obtained from the first and second time derivatives of the curve $a(t)$, respectively. This procedure enabled us to determine crack acceleration quantitatively. Generally it is not easy to obtain $\ddot{a}$ meaningfully from slopes of $\dot{a}$–t plots because data of $\dot{a}$ scatter significantly.

Figure 4 shows values of K_d, $\dot{a}$ and $\ddot{a}$ as a function of a. It should be noted that values of a giving the maximum $\dot{a}$ and K_d differed considerably. The maximum of $\dot{a}$ was attained earlier

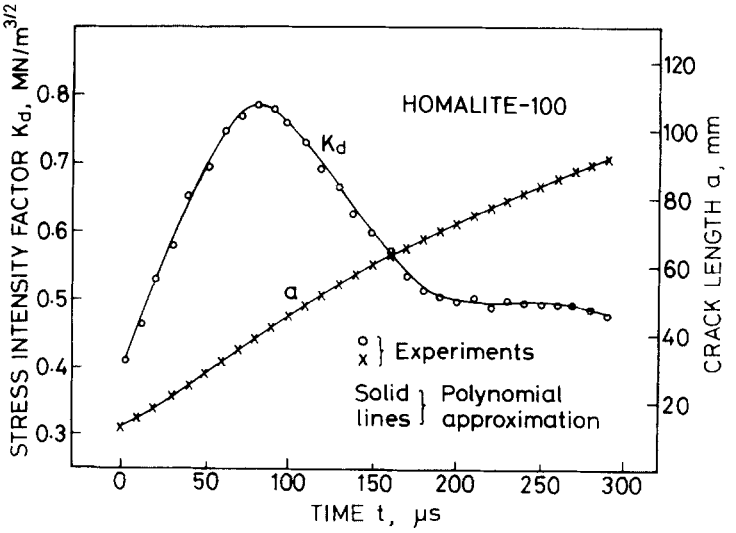

Fig. 3. Stress intensity factor K_d and crack length a for Homalite-100 as a function of time t.

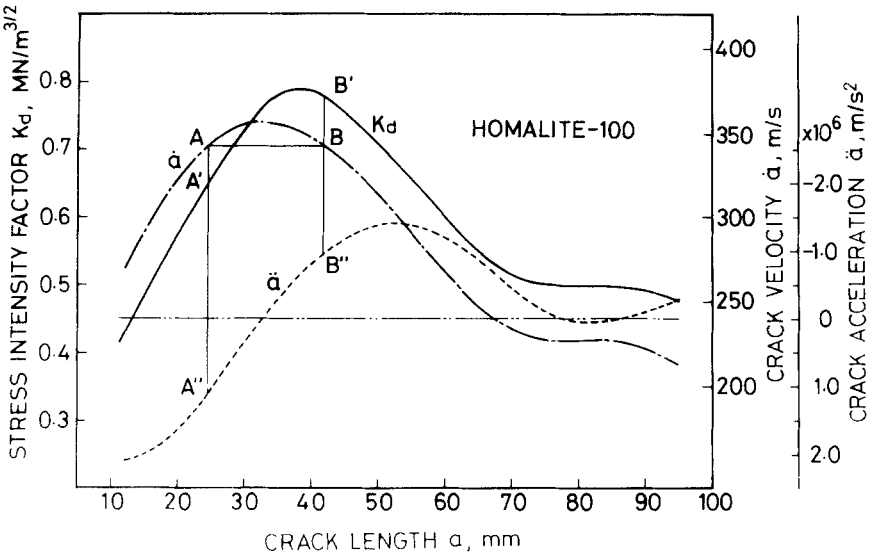

Fig. 4. Stress intensity factor K_d, crack velocity $\dot{a}$ and crack acceleration $\ddot{a}$ for Homalite-100 as a function of crack length a.

than the maximum of K_d. Such were the cases also with other Homalite-100 specimens tested.

3. Relation between stress intensity factor and crack velocity

The relation between K_d and $\dot{a}$ has been studied by several researchers to understand fracture behaviour of brittle materials [6, 10–15]. In the present work, the K_d–$\dot{a}$ relation was obtained for Homalite-100 to correlate it with fracture surface morphology. Figure 5 shows K_d–$\dot{a}$

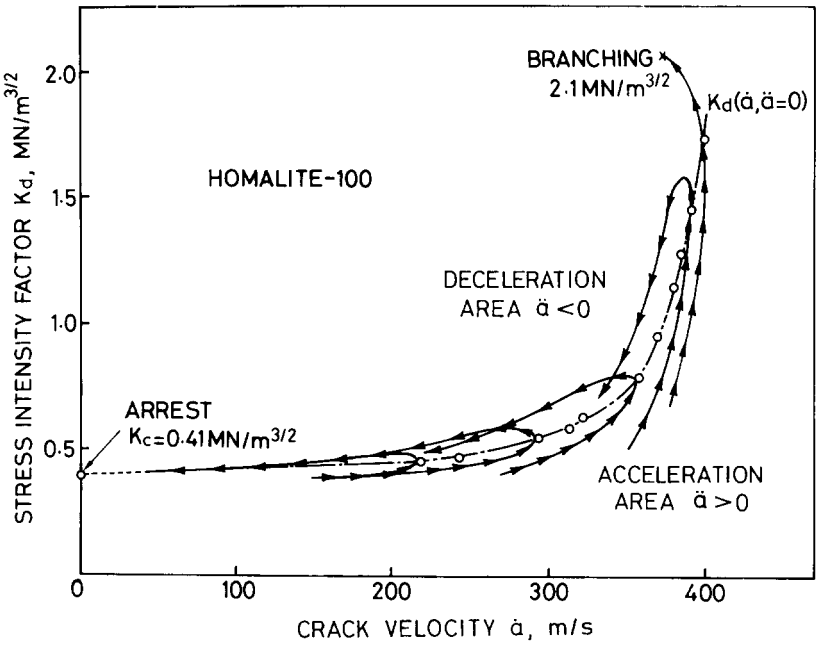

Fig. 5. Relation between stress intensity factor K_d and crack velocity $\dot{a}$ for Homalite-100.

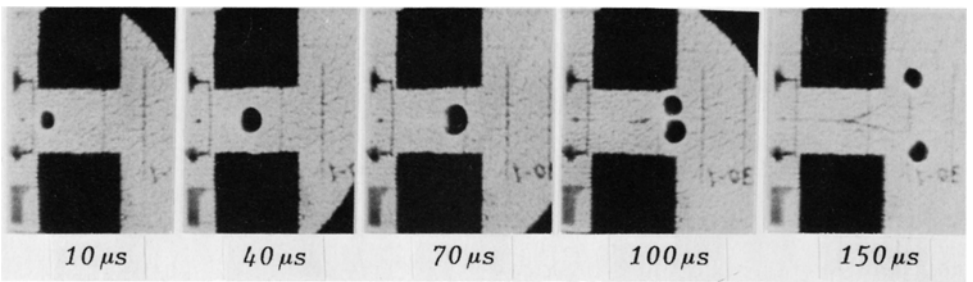

Fig. 6. Crack branching in a Homalite-100 specimen.

curves obtained from five specimens. The arrows indicate the progressing direction of fracture. The open circles represent the position of the peak velocities obtained from eleven specimens. The dotted curve of $K_d(\dot{a}, \ddot{a} = 0)$ was determined connecting these peak velocity points. Hence, this curve separates the acceleration and deceleration areas in the K_d–$\dot{a}$ diagram. It should be emphasized that K_d corresponding to a crack velocity was larger when the crack was decelerated than when it was accelerated (see also points A' and B' in Fig. 4). Similar results have also been obtained by the present authors for PMMA and epoxy specimens [6].

Figure 5 shows that there existed the minimum value of K_d at crack arrest, i.e., K_c whose value was $0.41\,\mathrm{MN\,m^{-3/2}}$.

Photographs showing crack branching in a Homalite-100 specimen are presented in Fig. 6. Branching occurred at $K_d = 2.1\,\mathrm{MN\,m^{-3/2}}$ and at $\dot{a} = 382\,\mathrm{m\,s^{-1}}$ (see Fig. 5). It is worth noting that the branching did not occur at the peak velocity but at the maximum value of K_d. Fracture surfaces became extremely rough prior to the branching, whereas they were very smooth just in advance of the arrest.

4. Morphological study for Homalite-100

4.1. Fracture markings

Figure 7 represents morphological features on a fracture surface of a Homalite-100 specimen which is the same as the one in Fig. 4. Two kinds of markings are remarkable here; line and tip markings. The former is due to the micro-level-difference formation, and the latter is considered to have resulted from secondary cracking which preceded the primary cracking [5]. Although no significant changes are seen in the number of line markings with the growing crack length, the pit density increased rapidly in an early stage and then decreased. This change is qualitatively in accord with the change in values of fracture parameters such as $\dot{a}$ and K_d (see Fig. 4). The relation between the pit density and $\dot{a}$ can be seen in more detail if one compares the two photographs at $a = 17$ mm and $a = 52$ mm. Although the crack velocities were nearly equal at both locations, the pit densities were obviously different; the higher density was obtained at $a = 52$ mm than at $a = 17$ mm. This may be attributed to the difference in values of K_d at the corresponding locations. The value of K_d was larger in the crack-decelerating area ($a = 52$ mm) than in the crack-accelerating area ($a = 17$ mm). On the other hand one may see the different relation between the pit density and K_d in two photographs at $a = 22$ mm and $a = 62$ mm, where there existed a great difference in the

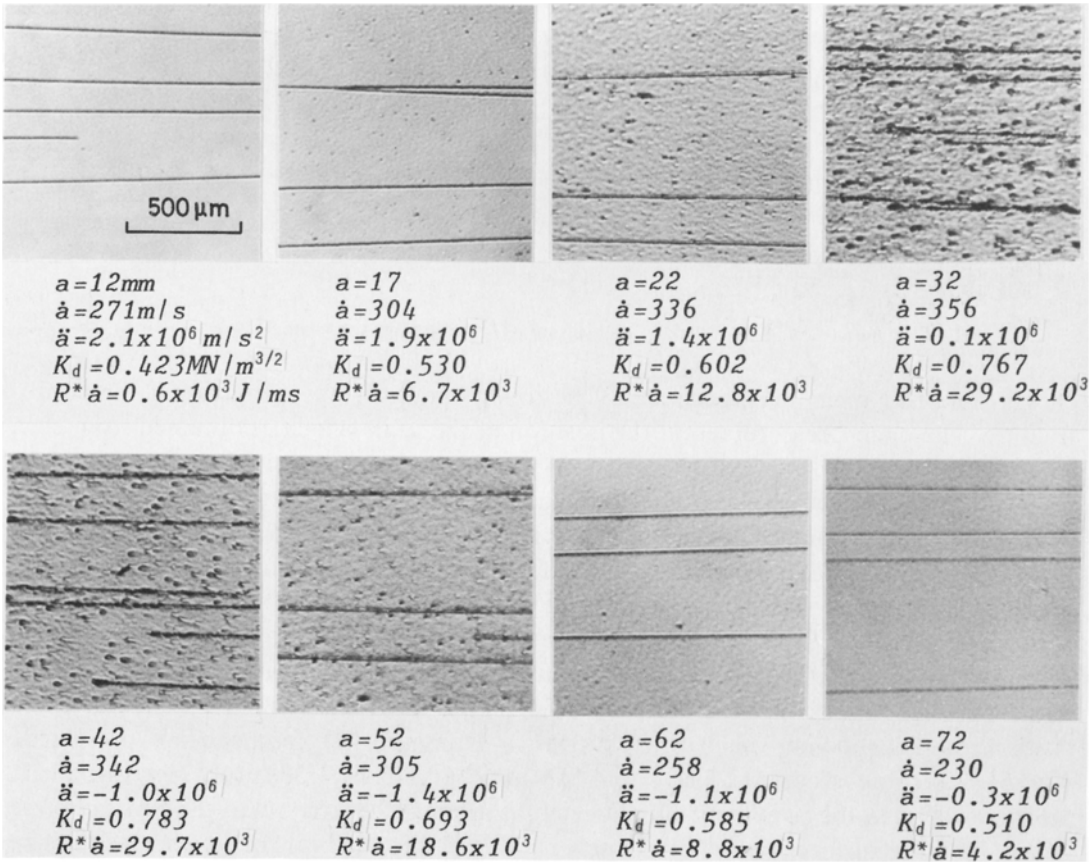

Fig. 7. Morphological change in fracture surface of Homalite-100.

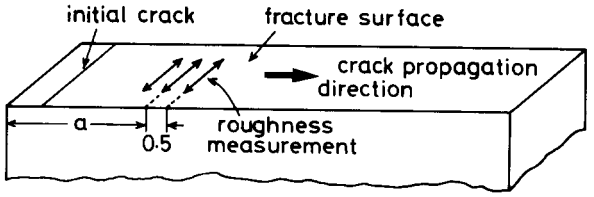

Fig. 8. Schematic view of roughness measurement.

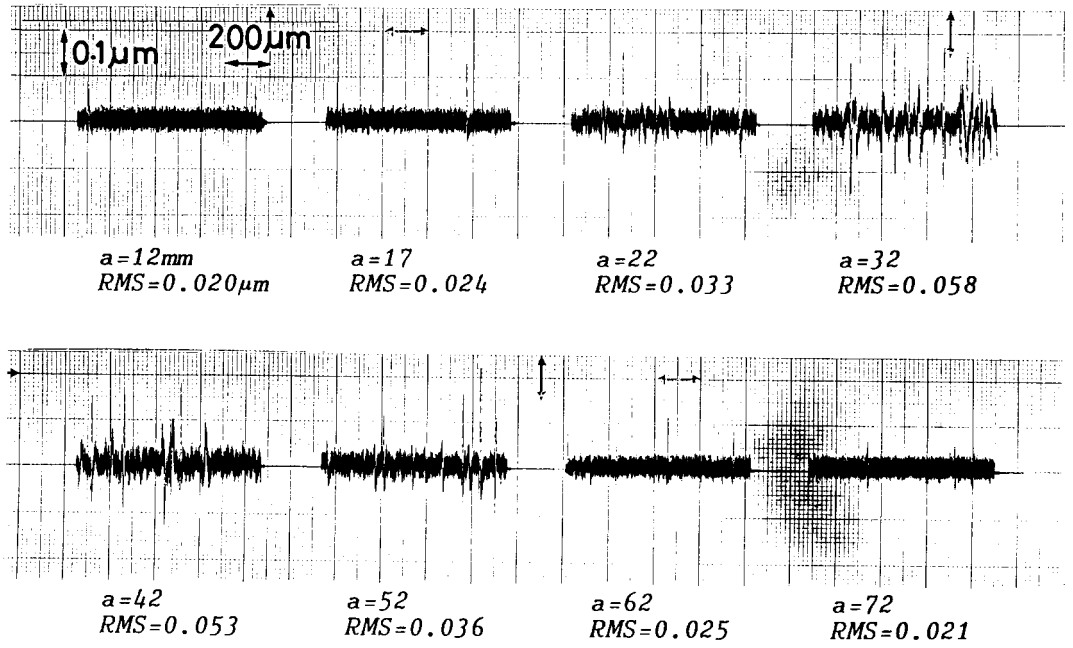

Fig. 9. Example of fracture surface profile of Homalite-100.

corresponding pit densities for almost the same values of K_d. A higher density was obtained in the higher crack velocity area (a = 22 mm) than in the lower crack velocity area (a = 62 mm). The results described above suggest that the pit density depends on both $\dot{a}$ and K_d, and that neither $\dot{a}$ nor K_d can be uniquely correlated with the density.

4.2. Measurement of fracture surface roughness

In order to relate quantitatively the fracture surface roughness with the other fracture parameters, a commercially available measuring instrument was used for the roughness measurement. Figure 8 illustrates a schematic view of a fractured specimen surface for the measurement which was carried out at an interval of 0.5 mm by scanning the surface with a needle (10 μm in tip radius) in a direction perpendicular to the direction of crack propagation. The measurement was limited to a central part of the fracture surface to avoid edge effects. Examples of the fracture surface profiles are shown in Fig. 9, where considerable roughness change is indicated with the advancement of the crack. In the present work, surface roughness was defined by the following equation:

$$\text{Root Mean Square Roughness (RMS)} = \left[\frac{1}{L}\int_0^L |f(x)|^2 \, \mathrm{d}x\right]^{1/2}, \tag{2}$$

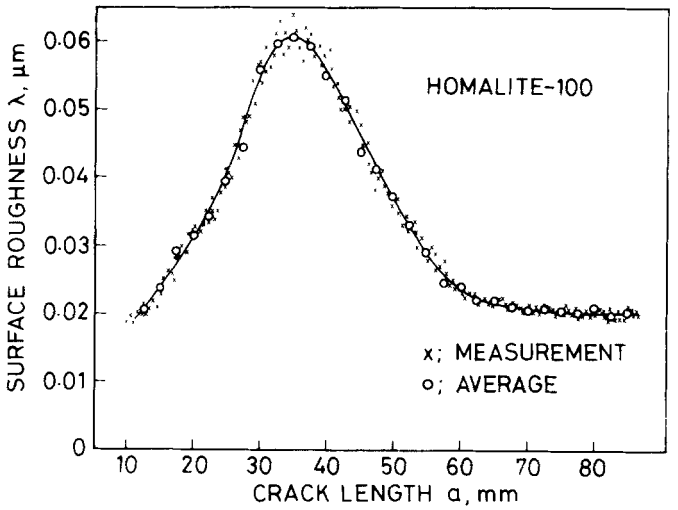

Fig. 10. Result of surface roughness measurement on Homalite-100.

where L is the scanned length and $f(x)$ is the roughness height at the point x. One may see a good correlation between the surface roughness change in Fig. 9 and the pit mark density change in Fig. 7. This intimate correlation may well be understood if one considers that generation of the pit marks is mostly responsible for the surface roughness in the present case.

Figure 10 shows the roughness distribution as a function of a, where each of the open circles was obtained on an average of eleven data belonging to every 5 mm-wide area (see Fig. 8). This averaged value λ is defined as the roughness at the area concerned. One may see that the change in $\lambda(a)$ is qualitatively in accord with the change in $\dot{a}(a)$ or $K_d(a)$ (see Fig. 4).

4.3. Relations between surface roughness and other fracture parameters

Figure 11 shows the relation between λ and $\dot{a}$. As suggested by Cotterell [3], λ has a close relation with $\dot{a}$. However, it is noted that λ cannot be uniquely correlated with $\dot{a}$; values of

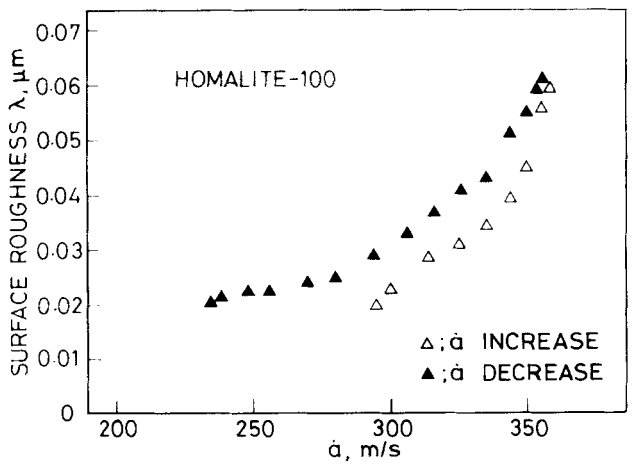

Fig. 11. Relation between surface roughness λ and crack velocity $\dot{a}$ for Homalite-100.

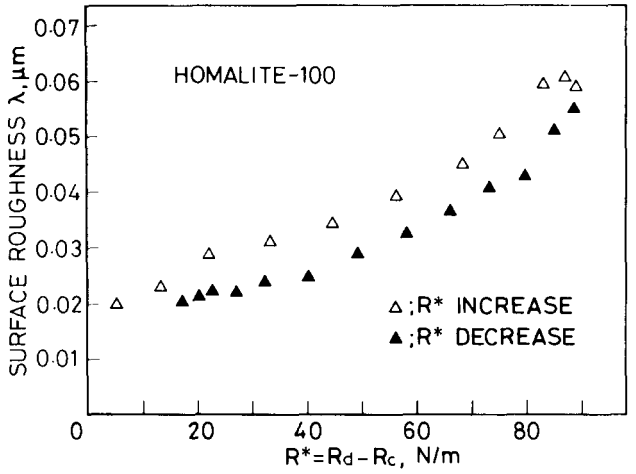

Fig. 12. Relation between surface roughness λ and specific crack extension resistance R^* for Homalite-100.

λ were larger when the crack was decelerated than when it was accelerated. This result is qualitatively well compared with that of K_d which was larger in a decelerating area than in an accelerating area at the same crack velocity.

The present authors consider that an inclement (R^*) of dynamic crack extension resistance (R_d) defined as follows:

$$R^* = R_d - R_c = (K_d^2 - K_c^2)/E_d \, [N/m] \tag{3}$$

should be responsible for the fracture roughness formation procedure, where K_d is considered to be larger than K_c. A similar parameter has been proposed by Maugis and Barquins [10] for understanding of fracture mechanics and adherence of viscoelastic bodies. Quantitatively, however, as shown in Fig. 12, a disparity existed between the two sets of data obtained from the R^*-increase and -decrease regions. The situation is opposite that in Fig. 11 where λ was larger in the $\dot{a}$-decrease region.

In order to explain the discrepancies described above, the authors have introduced a parameter $R^*\dot{a}$. Figure 13 shows how λ changes as a function of $R^*\dot{a}$. No great discrepancy

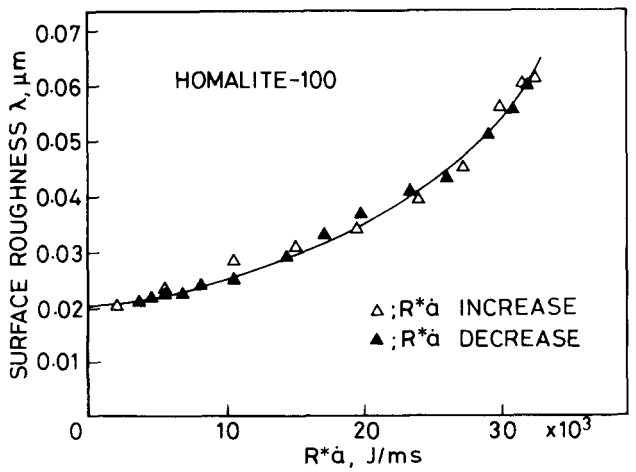

Fig. 13. Relation between surface roughness λ and product $R^*\dot{a}$ for Homalite-100.

existed between the two sets of data. One may see a good correlation also between $R^*\dot{a}$ and the density of the pit mark in Fig. 7. The physical meaning of $R^*\dot{a}$ is energy per unit crack width per unit time. A similar parameter has been used in theoretical analysis of dynamic crack propagation for calculation of the flow rate of energy into the crack tip region [16–19]. It seems very likely that this parameter plays an influential role in changing the fracture surface roughness and the pit mark density.

Fracture surfaces of Homalite-100 were relatively smooth when $\dot{a}$ was lower than 250 m s^{-1}, and over this velocity λ increased substantially. Such roughness change may well be understood if one looks at the K_d–$\dot{a}$ relations presented in Fig. 5. In the lower velocity region, the change in K_d was rather small and the product $R^*\dot{a}$ remained small resulting in relatively smooth surfaces, whereas in a higher velocity region $R^*\dot{a}$ increased significantly mostly due to the increase in K_d, and λ increased correspondingly. Fracture surfaces became extremely rough just before the crack branched. Thus, one may see that branching is likely to occur when $R^*\dot{a}$ attains a critical value. Such a view has been verified through experiments which were conducted on Araldite D by the present authors [20].

5. Morphological study for PMMA and epoxy

Experimental results obtained for PMMA and epoxy specimens are represented in Figs. 14 and 15, respectively. Those figures show relationships between λ and the parameters R^*, $\dot{a}$ and $R^*\dot{a}$. It is shown that crack lengths giving peak values of $\lambda(a)$ and $\dot{a}(a)$ differ from each other. There seems to exist a slight discrepancy also between crack lengths giving peak values of $\lambda(a)$ and $R^*(a)$: for the same roughness values which are indicated by points A and A', the corresponding values of $\dot{a}$ (see points B and B') or R^* (see points C and C') differed slightly. On the other hand, a good agreement is shown between crack lengths giving the peak values of $\lambda(a)$ and $R^*\dot{a}(a)$, and the values of $R^*\dot{a}$ are almost equal at points D and D' which correspond to points A and A', respectively. Figures 16 and 17 provide more detailed

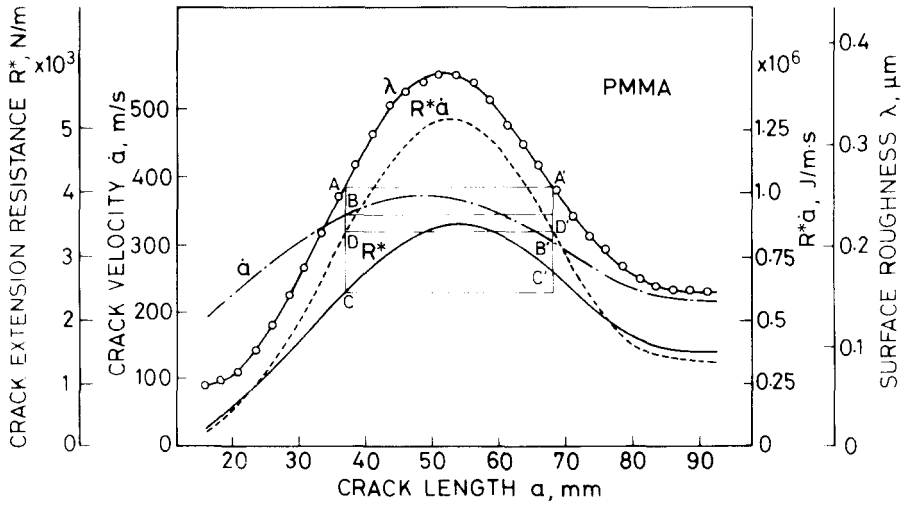

Fig. 14. Surface roughness λ, and specific crack extension resistance R^*, crack velocity $\dot{a}$ and product $R^*\dot{a}$ for PMMA as a function of crack length a.

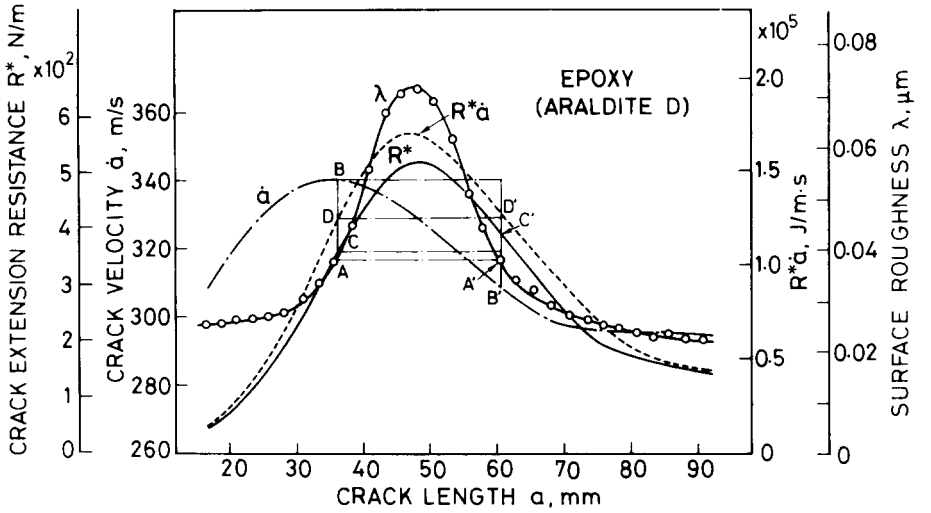

Fig. 15. Surface roughness λ, and specific crack extension resistance R^*, crack velocity $\dot{a}$ and product $R^*\dot{a}$ for epoxy as a function of crack length a.

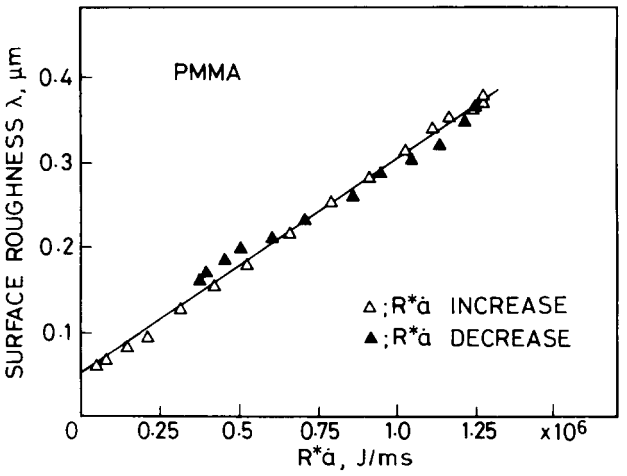

Fig. 16. Relation between surface roughness λ and product $R^*\dot{a}$ for PMMA.

relationships between λ and $R^*\dot{a}$ for PMMA and epoxy. It should be emphasized that there exists a good correlation between the two sets of data obtained in the $R^*\dot{a}$-increase and -decrease regions as was the case for Homalite-100. These results positively confirm the validity of employment of the parameter $R^*\dot{a}$ in interpretation of fracture surface morphology.

6. Conclusions

We measured crack velocity $\dot{a}$, acceleration $\ddot{a}$, stress intensity factor K_d and the specific crack extension resistance R^* during crack propagation in Homalite-100, PMMA and epoxy. Surface roughness measurements were also performed on the fracture surfaces. Conclusively

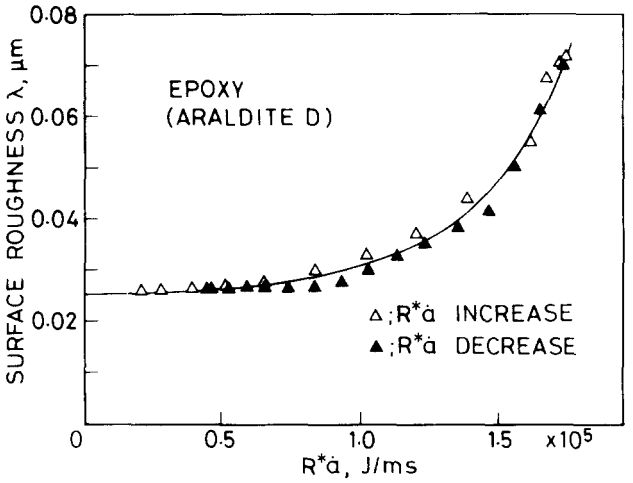

Fig. 17. Relation between surface roughness λ and product $R^*\dot{a}$ for epoxy.

it has been shown that the roughness had the best correlation with $R^*\dot{a}$ rather than with other parameters such as $\dot{a}$, K_d, and R^*.

References

1. J.W. Johnson and D.G. Holloway, *Philosophical Magazine* 14 (1966) 731–743.
2. M. Ramulu, A.S. Kobayashi, B.S.J. Kang and D.B. Barker, *Experimental Mechanics* 23 (1983) 431–437.
3. B. Cotterell, *Applied Materials Research* (October 1965) 227–232.
4. B. Cotterell, *The International Journal of Fracture Mechanics* 4 (1968) 209–217.
5. K. Ravi-Chandar and W.G. Knauss, *International Journal of Fracture* 26 (1984) 65–80.
6. K. Takahashi and K. Arakawa, *Experimental Mechanics* 27 (1987) 195–200.
7. H. Kolsky, *Stress Waves in Solids*, Oxford University Press, London (1952).
8. P. Manogg, dissertation, University of Freiburg, Germany (1964).
9. P. Manogg, *Glastech Berichte* 39 (1966) 323–329.
10. T. Kobayashi and J.W. Dally, *ASTM STP 627* (1977) 257–273.
11. A.S. Kobayashi and S. Mall, *Experimental Mechanics* 18 (1978) 11–18.
12. J.F. Kalthoff, in Workshop on Dynamic Fracture, California Institute of Technology (February 1983) 11–25.
13. K. Ravi-Chandar and W.G. Knauss, *International Journal of Fracture* 26 (1984) 141–154.
14. A.J. Rosakis and A.T. Zehnder, *International Journal of Fracture* 27 (1985) 169–186.
15. B.A. Crouch and J.G. Williams, *Engineering Fracture Mechanics* 26 (1987) 553–566.
16. D. Maugis and M. Barquins, *Journal of Physics D: Applied Physics* 11 (1978) 1989–2023.
17. J.W. Craggs, *Fracture of Solids*, D.C. Drucker and J.J. Gilman (eds.), Interscience Publishers (1962) 51–63.
18. J.D. Eshelby, in *Inelastic Behavior of Solids*, M.F. Kanninen et al. (eds.), McGraw-Hill (1970) 77–115.
19. G.C. Sih, in *Inelastic Behavior of Solids*, M.F. Kanninen et al. (eds.), McGraw-Hill (1970) 607–639.
20. K. Arakawa and K. Takahashi, in *Proceedings of the 6th International Congress on Experimental Mechanics* 2 (June 1988) 746–750.